

Parameter-free approximate equivariance for tasks with finite group symmetry

Riccardo Ali*, Pietro Liò† and Jamie Vicary‡

Department of Computer Science, University of Cambridge

16 May 2025

Abstract

Equivariant neural networks incorporate symmetries through group actions, embedding them as an inductive bias to improve performance on a wide variety of tasks. However, existing equivariant methods can be computationally intensive, with high parameter counts, and are often tied to a specific architecture. We propose a simple zero-parameter approach that imposes approximate equivariance for a finite group in the latent representation, as an additional term in the loss function. We conduct experiments which allow the network to learn a group representation on the latent space, and show in every case it prefers to learn the regular representation. Fixing this action on the latent space, this yields a simple method to impose approximate equivariance as an additional loss penalty. We benchmark our approach on three datasets and compare it against several existing equivariant methods, showing that in many cases it achieves similar or better performance for a fraction of the parameters.

1 Introduction

When we consider the problem of designing a neural network to solve a given task, we commonly observe the existence of a symmetry group G that acts naturally on the training data.¹ For purposes of discussion, we illustrate a generic architecture in Figure 1, which we interpret broadly: E may be any sort of feature extractor, such as in an encoder or classifier; and D may be any final component that produces outputs from latent representations, such as a classifier head or decoder. On the input and output layers, the representations ρ_X, ρ_Y may act geometrically, such as by rotation or flipping, or they may act non-geometrically by changing other aspects of the representation. Having trained our network to minimise the task loss in the usual way, we may consider to what extent the solution respects these actions. For example, we might expect an image classifier to have the property that transforming the input image leaves the output class *invariant* (in which case we would choose ρ_Y to act trivially.) For a different task such as an image-to-image pipeline, we might expect a more general *equivariant* behaviour, where transformations on the input layer yield corresponding nontrivial transformations on the output layer.

However, for certain tasks we can expect only *approximate equivariance*, where a transformation of the input vector corresponds inexactly, or nondeterministically, to a transformation of the outputs. This most general setup is typical of many real-world tasks, where we may encounter approximate

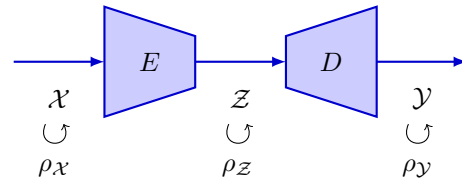


Figure 1: Generic architecture with input space \mathcal{X} , latent space \mathcal{Z} and output space \mathcal{Y} , carrying group actions ρ_X, ρ_Y on the input and output spaces, and potentially an action ρ_Z on the latent space.

*rma55@cam.ac.uk

†pl219@cam.ac.uk

‡jamie.vicary@cl.cam.ac.uk

¹We give a formal definition of a group action on a vector space (group representation) in Section 3.

scale-invariance of turbulent dynamics [10], approximate rotation-equivariance of turbulent smoke dynamics [9] (illustrated in Figure 2), and approximate reflection-invariance of pathologies in medical images [25]. The degree of approximation will depend heavily on the task.

A rich body of work in machine learning aims to design neural network architectures with improved performance for invariant, equivariant, or approximately equivariant tasks (see Section 2 for a brief survey.) Early work on Convolutional Neural Networks showed the power of translation invariance [15], and more recent methods have included Steerable Convolutional Neural Networks of Cohen and Welling [2] which allow rotationally-invariant filters, and Residual Pathway Priors due to Finzi, Benton and Wilson [5] which use residual connections as a mechanism for approximate equivariance. These and other methods achieve impressive performance on a variety of datasets, albeit typically at the cost of high model complexity, increased training times, and significantly elevated parameter counts compared to baseline architectures.

In our work we consider a perspective which is relatively under-studied: allowing a group action ρ_Z on the latent space (see Figure 1). We exhibit experimental results that demonstrate a unique such choice of representation, which for a variety of tasks and architectures, is able to maximise the degree of equivariance between the input, latent and output layers. Fixing this unique representation, and selecting a suitable loss function, we arrive at a new lightweight training regime, with strong performance on a variety of invariant, equivariant and approximately-equivariant tasks.

In summary, we present the following contributions.

- We present a new method for training neural networks to solve invariant, equivariant and approximately-equivariant tasks where a finite group acts on the input and output spaces. Our method is conceptually simple, and adapts easily to any neural network architecture.
- We use a single tunable parameter, and no additional learnable parameters, compared to alternative approaches which typically have large learnable parameter demands, in some cases 5-20 times baseline.
- Our method uses the regular group representation on the latent space, which we experimentally motivate by showing that the system prefers to learn this representation in a variety of example tasks.
- We show that our method is competitive with or exceeds state-of-the art in a range of benchmarks, with lower computational budget than many other high-performing methods.

The rest of the paper is structured as follows. Sections 2 and 3 describe similar efforts and introduce group representations. Section 4 describes our studies to determine the optimal representation on the latent space. Section 5 describes our new methodology, and Section 6 presents the main experimental results. Finally, Section 7 suggests possible future work, and Section 8 contains concluding remarks.

2 Related Work

A wide variety of methods have been developed to train neural networks to solve tasks in the presence of invariance, equivariance, or approximate equivariance. We give a brief summary here of those methods which are most relevant for our present work.

One of the most studied bodies of work derive from Convolutional Neural Networks (CNNs), which of course have strict translation invariance in their traditional form [15, 18]. Weiler and collaborators employ the framework of steerable functions [7] to construct a rotation-equivariant Steerable CNN architecture (SCNN) [2], which strictly respects both translation and rotation equivariance; this was later generalised to develop a theory of general $E(2)$ -equivariant steerable

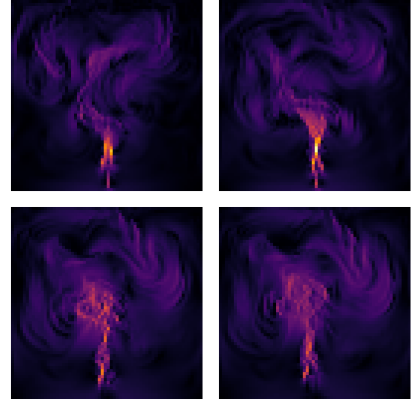


Figure 2: Approximately-equivariant dynamics of smoke plumes [9].

CNNs (**E2CNN**), which allow the degree of equivariance to be controlled by explicit choices of irreducible representation of the symmetry group [24]. Such a network can avoid learning redundant rotated copies of the same filters. Wang, Walters and Yu, utilise steerable filters to obtain convolution layers with approximate translation symmetry and without rotation symmetry (**RSteer**), and with approximate translation and rotation symmetry (**RGroup**) [21]. These authors relax the strict weight tying of E2CNNs, replacing single kernels with weighted linear combinations of a kernel family, with coefficients that are not required to be rotation- or translation-invariant. An third approach named Probabilistic Steerable CNNs (**PSCNN**) was proposed recently by Veeffkind and Cesa [19], which allows SCNNs to determine the optimal equivariance strength at each layer as a learnable parameter. All these methods have demonstrated enhanced performance on a variety of tasks, albeit at the cost of increased training time and model complexity. They all require a significant increase in the number of learnable parameters compared to baseline (see parameter comparison in Section 6.)

We also discuss a family of approaches which are not based around the CNN architecture. Residual Pathway Priors (**RPP**), due to Finzi et al [5], is a model where each layer is effectively doubled, yielding a first layer with strong inductive biases, and a second layer which is less constrained, with final output is obtained as the sum of these layers. Another architecture is Lift Expansion (**LIFT**), which factorizes the input space into equivariant and non-equivariant subspaces, and applies different architecture to each [20]; this approach works by tiling a non-equivariant encoder across the equivariant dimensions. We also consider prior work on learning equivariant representations. Dupont et al. [4] proposed a parameter-free method to learn equivariant neural implicit representations for view synthesis; while similar to our method in some respects, their work strongly leverages the defining representation of the infinite group $O(3)$, is limited to latent spaces with the same geometrical structure as the input space, and does not apply to arbitrary latent encodings. Jin et al. [12] present a similar method which learns non-linear group actions on the latent space using additional learnable parameters, augmented by an optional attention mechanism; in contrast, in our model the group acts linearly on the latent space with a fixed representation, with no additional parameters required.

3 Background on groups and their representations

Here we outline the essential aspects of representation theory for finite groups which we will use in the paper. All results presented here are standard, and we do not give citations for specific results; for more information we recommend the standard texts by Fulton and Harris [6] and James and Liebeck [11]. We work over a base field \mathbb{K} which is assumed to be \mathbb{R} or \mathbb{C} , and we assume the group G is finite; some results we state rely on these assumptions.

Groups. A group G is a set equipped with an associative and unital binary operation, such that every element has a unique inverse. Important families of groups include the following. The dihedral group D_n is the group of symmetries of the regular polygon with n sides. For $n > 2$ this is intuitively clear; the group D_1 is the group with 2 elements. The cyclic group C_n is the groups of integers $\{0, \dots, n-1\}$ with addition modulo n . The permutation group S_n is the group of permutations of an n -element set. We may define groups by presentations, which give generators and relations for the product; for example, the group D_1 can be defined by the presentation $\{1, a \mid a^2 = 1\}$. For any two groups G, H , we write $G \times H$ for the product group, whose elements are ordered pairs of elements of G and H respectively.

Representations. A *representation* or *action* ρ of a finite group G on a vector space \mathcal{V} is a choice of linear maps $\rho(g) : \mathcal{V} \rightarrow \mathcal{V}$ for all elements $g \in G$, with the property that $\rho(e) = \text{id}_{\mathcal{V}}$ for the identity element $e \in G$, and such that $\rho(g)\rho(g') = \rho(gg')$ for all pairs of elements $g, g' \in G$. We define the *dimension* of ρ to be $\dim(\mathcal{V})$, the dimension of the vector space \mathcal{V} . There is a notion of equivalence of representations: given representations ρ on \mathcal{V} , and ρ' on \mathcal{V}' , they are *isomorphic* when there is an invertible linear map $L : \mathcal{V} \rightarrow \mathcal{V}'$ such that $L\rho(g) = \rho'(g)L$ for all $g \in G$. Given a subgroup $G \subseteq G'$, a representation of G' yields a *restricted representation* on G in an obvious way.

Some simple examples of representations include the *zero representation* on the zero-dimensional vector space, and the *trivial representation* ρ_{triv} on the 1-dimensional vector space \mathbb{K} , where $\rho_{\text{triv}}(g) = \text{id}_{\mathbb{K}}$ for all $g \in G$. For the case of a finite group, a more interesting representation is the

regular representation ρ_{reg} . To construct this, we first define $\mathbb{K}[G]$ as the *free vector space* generated by G ; elements of this vector space are linear combinations of group elements $\sum_i c_i g_i$ weighted by coefficients $c_i \in \mathbb{K}$. As a vector space, this can also be written $\mathbb{K}^{|G|}$, the cartesian product of $|G|$ copies of the base field. Then ρ_{reg} is defined as a representation on $\mathbb{K}[G]$ as follows:

$$\rho_{\text{reg}}(g)(\sum_i c_i g_i) = \sum_i c_i (gg_i) \quad (1)$$

By construction we have $\dim(\rho_{\text{reg}}) = |G|$, the size of the group. A representation ρ on the vector space \mathbb{K}^n is a *permutation representation* when for all $g \in G$, the matrix $\rho(g)$ is a permutation matrix. By construction, the regular representation is a permutation representation.

Permutation groups S_n have a particularly rich representation theory. Every permutation group has a sign representation ρ_{sign} on \mathbb{K} , defined as $\rho_{\text{sign}}(g) = +1$ for an even permutation, and -1 for an odd permutation. A permutation group also has a *standard representation* ρ_{std} on \mathbb{K}^{n-1} , defined as the regular representation restricted to the subspace of vectors with coefficients that sum to zero. For groups which embed into S_n in an obvious way, such as D_n , we can also talk about sign and standard representations, which are defined by restriction.

Irreducibility. Given vector spaces V and V' we can form their direct sum $V \oplus V'$, with elements which are ordered pairs of elements (v, v') of V and V' respectively. Given a representation ρ on V , and ρ' on V' , we can form their *direct sum* $\rho \oplus \rho'$ acting on the vector space $V \oplus V'$, as follows:

$$(\rho \oplus \rho')(g)(v, v') := (\rho(g)(v), \rho'(g)(v')) \quad (2)$$

For an integer n , we can similarly define the *n-fold multiple* of ρ , written $n \cdot \rho$, as $\rho \oplus \rho \oplus \dots \oplus \rho$. If $\rho = \rho' \oplus \rho''$, we say that ρ' and ρ'' are *subrepresentations* of ρ .

A representation is *irreducible* if it is not isomorphic to a direct sum of other representations, except for itself and the zero representation. Any finite group has a finite number of irreducible representations up to isomorphism. For example, the group S_2 has just the trivial and sign representations; the group S_3 , has just the trivial, sign and standard irreducible representations (with the same for D_3 as they are isomorphic as groups); and the cyclic group C_n has n irreducible representations over \mathbb{C} , one corresponding to each n th root of unity.

Orthogonality of representations. For a fixed group G , it is interesting to ask whether a representation ρ contains an irreducible representation ρ' as a direct summand, and if so with what multiplicity. This can be determined using the formula for *inner product of representations*:

$$\langle \rho, \rho' \rangle = \frac{1}{|G|} \sum_{g \in G} \overline{\text{Tr}(\rho(g))} \text{Tr}(\rho'(g)) \quad (3)$$

Given the knowledge of all irreducible representations of a finite group, this method allows us to determine their multiplicities as subrepresentations of ρ . This sequence of natural numbers determines ρ up to isomorphism.

4 Identifying optimal representations on the latent space

We suppose a network architecture as illustrated in Figure 1 is given, with training set $(x_i, y_i) \in \mathcal{X} \times \mathcal{Y}$, and task loss $L_{\text{task}}(D(E(x_i)), y_i)$. In the usual way, such a network may be trained with backpropagation using the task loss as an objective function, to learn suitable parameters for the network components E and D . We now suppose a finite symmetry group G is specified, which acts by fixed representations $\rho_{\mathcal{X}}, \rho_{\mathcal{Y}}$ on the input and output spaces respectively. We are interested to answer the following question: if we use additional learnable parameters to construct a third representation $\hat{\rho}_{\mathcal{Z}}$ of G on the latent space \mathcal{Z} , which we co-train alongside the parameters for E, D with a suitable loss function, what representation $\hat{\rho}_{\mathcal{Z}}$ does the model prefer to learn? To investigate this, we conduct experiments with the following loss function:

$$\begin{aligned} L_{\text{opt}} = & L_{\text{task}}(D(E(x_i)), y_i) & (i) \text{ Task loss} \\ & + \lambda_t L_{\text{task}}(D(\hat{\rho}_{\mathcal{Z}}(g)(E(x_i))), \rho_{\mathcal{Y}}(g)(y_i)) & (ii) \text{ Equivariance loss between } \rho_{\mathcal{Z}} \text{ and } \rho_{\mathcal{Y}} \\ & + \lambda_e \text{MSE}(\hat{\rho}_{\mathcal{Z}}(g)(E(x_i)), E(\rho_{\mathcal{X}}(g)(x_i))) & (iii) \text{ Equivariance loss between } \rho_{\mathcal{X}} \text{ and } \rho_{\mathcal{Z}} \\ & + \lambda_a (\text{ALG}_{G,d} + \text{REG}_{G,d}) & (iv) \text{ Algebra loss} \end{aligned}$$

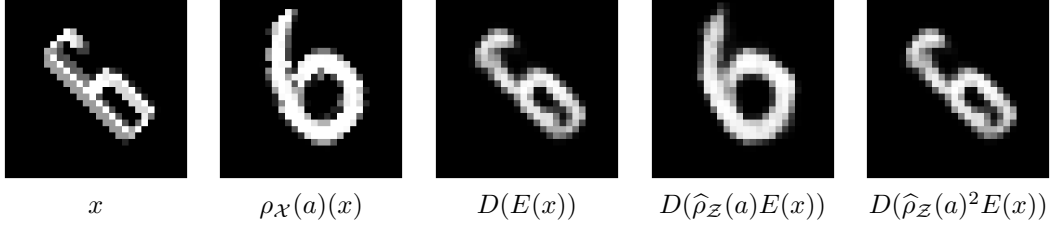


Figure 3: Visualisation of our learned encoder E , decoder D and latent action $\hat{\rho}_Z$ on input vector x .

We motivate this loss function as follows. Component (i) ensures that E, D are appropriately trained for the underlying task. Component (ii) encourages E, D to be equivariant with respect to the learned action $\hat{\rho}_Z$ on the latent space and the fixed action ρ_Y on the output space. This component re-uses the underlying task loss function. Component (iii) encourages E to be equivariant with respect to the fixed representation ρ_X on the input space and the learned representation $\hat{\rho}_Z$ on the latent space. This component uses MSE rather than the task loss function, since it is defined on feature vectors in the latent space, rather than the output space.² Component (iv) is a penalty term which packages together the necessary algebraic properties for $\hat{\rho}_Z$ to become a high-quality representation of G ; it includes a first part $\text{ALG}_{G,d}$ arising from the group presentation, and a second regularisation term $\text{REG}_{G,d}$.

To give further insight into component (iv), suppose our goal is to learn a representation $\hat{\rho}_Z$ of the group D_1 , which has group presentation $\{1, a \mid a^2 = 1\}$. Then $\hat{\rho}_Z$ should satisfy $\hat{\rho}_Z(a) = \text{id}$ and $\hat{\rho}_Z(a)\hat{\rho}_Z(a) = \text{id}$. To achieve this, we fix the parameter $\hat{\rho}_Z(a) = \text{id}$, and choose $\text{ALG}_{D_1,d}$ and $\text{REG}_{D_1,d}$ as follows, where $d = \dim(\mathcal{Z})$, the matrix Id_d is the identity of size $d \times d$:

$$\text{ALG}_{D_1,d} = \text{MSE}(\hat{\rho}_Z(a)^2, \text{Id}_d) \quad \text{REG}_{D_1,d} = \text{MSE}(\hat{\rho}_Z(a), \hat{\rho}_Z(a)^{-1})$$

We note that when $\text{ALG}_{D_1,d}$ equals zero then $\hat{\rho}_Z(a)^2 = \text{Id}_d$, and hence $\text{REG}_{D_1,d}$ will equal zero. In this sense, the regularisation term is algebraically redundant. However, it changes the loss landscape in a way that significantly improves convergence, in this case by controlling the behaviour of the inverse $\hat{\rho}_Z(1)^{-1}$. Full details of the regularisation terms are given in the technical appendix.

Suppose we are able to train a good solution with respect to L_{opt} , which in particular achieves good scores on component (iv), so that $\hat{\rho}_Z$ is a true group-theoretic representation to high accuracy. We may then use techniques from representation theory to analyze what representation the model has learned. We explore this in toy settings with the MNIST [3], TMNIST [16] and CIFAR10 [14] datasets, for both autoencoder and classifier tasks, and for the groups D_1, D_3 and C_4 . As this procedure is architecture-agnostic, we are able to use both CNN- and MLP-based architectures. All these experiments support the same conclusion: the model prefers to learn a representation $\hat{\rho}_Z$ which is isomorphic to some multiple of the regular representation of G .

4.1 TMNIST autoencoder, CNN architecture, $G = D_1$

For our first experiment we use the TMNIST dataset, of digits rendered in a variety of typefaces. We choose a subset of two typefaces only, producing 20 images, and we augment with arbitrary rotations and scaling. For our group we choose $G = D_1$ presented as $\{1, a \mid a^2 = 1\}$. Since this is an autoencoder we have $\mathcal{X} = \mathcal{Y}$, and we choose $\rho_X = \rho_Y$, with the nontrivial element $\rho_X(a) = \rho_Y(a)$ acting to flip the choice of font, with rotation and scaling left invariant.

For the algebra loss component (iv) we choose $\text{ALG}_{D_1,d} = \text{MSE}(\hat{\rho}_Z(a)^2, \text{Id}_d)$ where $d = \dim(\mathcal{Z}) = 42$.

We present our findings in Figure 1, with each run giving one row of the table, and we give a visualisation in Figure 3. Low values in the algebra loss and equivariance loss columns show that we learn high-quality representations $\hat{\rho}_Z$, which are strongly equivariant with respect to the

²In the presence of G -augmentation, components (i)-(iii) are strongly related. In particular, if component (iii) is perfectly satisfied, then we may conclude $\hat{\rho}_Z(g)(E(x_i)) = E(\rho_X(g)(x_i))$, and component (ii) then becomes proportional to $L_{\text{task}}(D(E(\rho_Y(g)(x_i))), \rho_Y(g)(y_i))$, a g -shift of the task loss component (i).

Table 1: TMNIST autoencoder task, learned representations of D_1 on latent space.

Run	Irreducible counts		Algebra loss	Equivariance loss
	-1	+1		
1	22	20	2.55×10^{-7}	5.70×10^{-3}
2	21	21	1.53×10^{-5}	1.36×10^{-2}
3	22	20	1.51×10^{-6}	1.24×10^{-2}
4	21	21	1.07×10^{-6}	1.27×10^{-2}
5	21	21	1.96×10^{-6}	1.49×10^{-2}

representations ρ_X, ρ_Y . By mapping the eigenvalues of $\hat{\rho}_Z(a)$ to the nearest value in $\{-1, +1\}$, we can determine the corresponding irreducible representation. By inspection we see that our learned representations contain the +1 and -1 representations with approximately equal multiplicity, and hence to good approximation $\hat{\rho}_Z$ is a multiple of the regular representation of D_1 .

4.2 MNIST autoencoder, MLP architecture, $G = D_3$

For our second experiment we choose the MNIST dataset of handwritten digits, augmented by arbitrary rotations. We choose the group $G = D_3$, the group of symmetries of an equilateral triangle. We choose generators r, s , with action on the input space and output space such that r acts as a clockwise 120-degree rotation, and s acts as a flip about the vertical axis. With these generators, the group D_3 has the following presentation: $\{e, r, r^2, r^3, s, rs \mid r^3 = e, s^2 = e, rsrs = e\}$. We parameterize the linear maps $\hat{\rho}_Z(r)$ and $\hat{\rho}_Z(s)$ independently, and define the following algebra loss, where $d = \dim(Z) = 30$, and where summands correspond to constraints in the presentation:

$$\text{ALG}_{D_3, d} = \text{MSE}(\hat{\rho}_Z(r)^3, \text{I}_d) + \text{MSE}(\hat{\rho}_Z(s)^2, \text{I}_d) + \text{MSE}(\hat{\rho}_Z(r)\hat{\rho}_Z(s)\hat{\rho}_Z(r)\hat{\rho}_Z(s), \text{I}_d) \quad (4)$$

We present our results in Figure 2. Since we are working with a nonabelian group, we cannot identify the representation by looking only at eigenvalues, and we use the representation inner product method of Section 3 to determine the multiplicities of the irreducible subrepresentations. The data shows that to high accuracy we learn representations containing trivial, sign and standard irreducible representations with multiplicities in the ratio 1:1:2, as expected for a multiple of the regular representation of D_3 . We also illustrate in Figure 4 the dynamics of the eigenvalues of $\hat{\rho}_Z(r)$, which shows them clustering evenly during training around the third roots of unity, despite an uneven initialization.

Table 2: MNIST autoencoder task, learned representations of D_3 on latent space.

Run	Irreducible counts			Algebra loss	Equivariance loss
	Trivial	Sign	Standard		
1	5.017	4.992	09.99	5.90×10^{-3}	2.2×10^{-2}
2	6.471	4.752	09.39	6.82×10^{-3}	1.9×10^{-2}
3	5.004	4.193	10.40	5.30×10^{-3}	2.0×10^{-2}
4	4.960	4.928	10.06	5.68×10^{-3}	1.8×10^{-2}
5	5.021	4.990	09.99	8.35×10^{-4}	2.2×10^{-2}

4.3 CIFAR10 classifier, CNN architecture, $G = C_4$

This experiment uses the CIFAR10 image dataset [14], containing 60,000 32×32 coloured images of everyday items organised in 10 classes. We choose the group $G = C_4$ of 90-degree rotations, with the algebraic loss function $\text{ALG}_{C_4, d} = \text{MSE}(\hat{\rho}_Z(1)^4, \text{I}_d)$, where $d = \dim(Z) = 64$. We present our results in Figure 3. As for previous experiments, this demonstrates that to high accuracy we are learning representations which are multiples of the regular representation of C_4 .

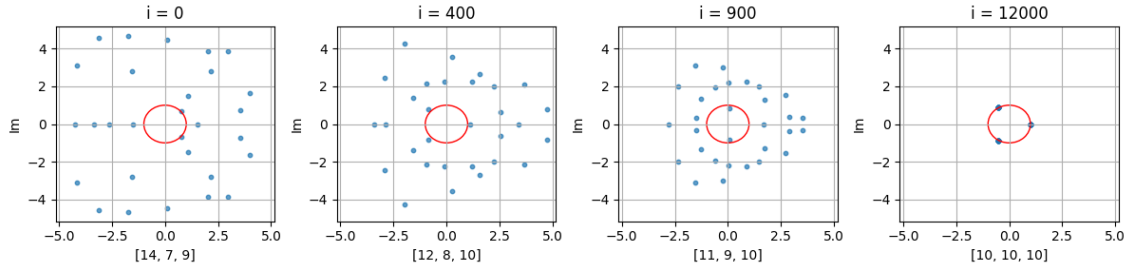


Figure 4: Complex eigenvalues of the real-valued matrix $\hat{\rho}_Z(r)$ in the D3 experiment, visualised at different training epochs. Beneath each plot we show counts of the nearest eigenvalues to each third root of unity.

Table 3: CIFAR classifier task, representations of C_4 learned on latent space.

Run	Irreducible counts				Algebra loss	Equivariance loss
	+1	+i	-1	-i		
1	16	16	16	16	4.02×10^{-5}	2.1×10^{-2}
2	16	16	16	16	5.74×10^{-5}	1.1×10^{-2}
3	15	17	15	17	3.04×10^{-5}	1.2×10^{-2}
4	16	16	16	16	5.82×10^{-5}	1.2×10^{-2}
5	16	15	18	15	4.99×10^{-5}	1.2×10^{-2}

5 Method

We present a novel parameter-free method to improve performance of neural networks to solve a variety of invariant, equivariant or approximately equivariant tasks, where a finite group G acts on the input and output layers with representations ρ_X and ρ_Y respectively. Inspired by the results of Section 4, we now fix the representation ρ_Z on the latent layer to be a multiple of the regular representation of G , with chosen multiplicity n . Where $n|G| < \dim(\mathcal{Z})$, we pad by taking the direct sum with additional copies of the trivial representation, to ensure our representation on \mathcal{Z} has the correct dimension. More precisely, our proposed representation is:

$$\rho_Z := n \cdot \rho_{\text{reg}} \oplus \max(\dim(\mathcal{Z}) - n|G|, 0) \cdot \rho_{\text{triv}} \quad (5)$$

Our method is intended to be used in the case where $\dim(\mathcal{Z}) \geq |G|$, so that at least one copy of the regular representation can be included. When the latent space is structured, for example as a product of features and channels, we choose an isomorphic form of the regular representation that preserves this structure (an example is given in Section 6.3). We then train according to the following objective function, where $(x_i, y_i) \in \mathcal{X} \times \mathcal{Y}$ is an element of the training set, $g \in G$ is a group element, and $L_{\text{task}}(x_i, y_i)$ is the original task loss function:

$$\begin{aligned}
& \frac{1}{2} L_{\text{task}}(D(E(x_i)), y_i) && \text{Task loss} \\
& + \frac{1}{2} L_{\text{task}}(D(E(\rho_X(g)(x_i))), \rho_Y(g)(y_i)) && \text{Task loss shifted by } g \\
& + \lambda \text{MSE}(E(\rho_X(g)(x_i)), \rho_Z(g)(E(x_i))) && \text{Equivariance loss from input to latent layer}
\end{aligned}$$

When used in a training loop we select (x_i, y_i) and g uniformly at random. Here λ is a hyperparameter expressing strength of the equivariance loss. Our model has no additional learned parameters above baseline, since the representation ρ_Z is now fixed. Our use of the g -shifted task loss means that our training dataset must be augmented by the action of G .

6 Experiments

We benchmark our method against a variety of state-of-the-art methods for three distinct tasks. These are: double-digit MNIST classification with independent transformation of the digits,

Table 4: Higher is better. DDMNIST test accuracies for different models and symmetry groups. We show mean accuracy over 5 runs, with the std. dev. in brackets. Parameter counts are given, and data augmentation is used in all runs. The best statistic in each column is in bold.

Model	Aug	C_4	Par (M)	D_1	Par (M)	D_4	Par (M)
CNN	Yes	0.907 (0.004)	0.03	0.938 (0.006)	0.03	0.800 (0.001)	0.03
SCNN	Yes	0.484 (0.008)	0.12	0.474 (0.003)	0.03	0.431 (0.010)	0.15
Restriction	Yes	0.914 (0.007)	0.12	0.890 (0.007)	0.33	0.837 (0.020)	0.17
RPP	Yes	0.908 (0.022)	0.79	0.903 (0.009)	0.08	0.827 (0.020)	1.73
PSCNN	Yes	0.909 (0.007)	0.51	0.871 (0.016)	0.04	0.842 (0.011)	1.23
Ours	Yes	0.915 (0.004)	0.03	0.947 (0.004)	0.03	0.868 (0.002)	0.03

using symmetry groups C_4 , D_4 and D_1 ; classification of Organ, Synapse and Nodule subsets of MedMNIST3D, using symmetry group S_4 ; an autoregression task for predicting smoke dynamics with symmetry group is C_4 . We compare our results against the models SCNN, E2CNN, LIFT, RPP, RGroup, RSteer, and PSCNN, which are all described in Section 2.

All our experiments follow the setup of the original papers as far as possible. For the runs of our method that we report, the learning rate and the equivariance hyperparameter λ have been tuned. All runs for our method use a lower or equal computational budget than required for training the other models. Since our method requires augmentation of training data, we give both augmented and unaugmented CNN baselines where possible, and we also indicate clearly in results tables where augmentation has been used for the training dataset. Full technical details for all our reported runs, as well as our chosen hyperparameters, are reported in the technical appendix. The ablation needed to demonstrate effectiveness of our method is comparison with the augmented CNN baseline. Experimental results are given in Figures 4, 5 and 6, and include parameter counts. In the majority of cases our results are improved or comparable with state-of-the-art, while using only a fraction of the parameters. Our method does perform less well in some cases, and we comment on that below.

6.1 Classification Task, DDMNIST, $G = C_4, D_1, D_4$

For each of the chosen symmetry groups C_4 , D_1 and D_4 , we randomly and independently transform two MNIST 28×28 digits according to the group. The group C_4 acts by 90-degree rotations, the group D_1 acts by reflection about horizontal axis, and the group D_4 acts by reflections and 90-degree rotations. We concatenate the two images horizontally and add padding to obtain a 56×56 image, and augment with noise, following the setup of Veefkind and Cesa [19]. Full details are given in the technical appendix. Because the transformations are local and independent, we apply our method using the product group; for example, if the symmetry group D_4 is used to transform the numerals, our method will use the regular representation of $D_4 \times D_4$.

Table 4 shows classification accuracies on DDMNIST for the different models and groups where, for each column, SCNN, Restriction, RPP and PSCNN are equivariant to the group in that column. The nature of the task means that training sets are augmented for all models. Except for SCNN, we re-trained and re-evaluated all models using almost the same setup as the original authors [19], using publicly available code. Our setup has the following differences. Firstly, we use a different learning rate for the CNN model, as we found that this increased performance and ensured a more meaningful baseline comparison. Secondly, we increased the number of filters in the penultimate layer from 48 to 66, so that it was large enough to contain a copy of the regular representation of $D_4 \times D_4$, which is a requirement of our method. For all other models this marginally improved performance, and we give the improved results here. Our method outperforms other architectures across all symmetry groups, despite having fewer parameters.

6.2 Classification Task, MedMNIST3D, $G = S_4$

We test our method on the Organ, Synapse and Nodule subsets of the MedMNIST3D dataset, using the same setup as the original authors [19]. We apply the octahedral group of orientation-preserving

symmetries of the cube, which is isomorphic to the permutation group S_4 . All results, except for ours and the augmented CNN, are imported from the original authors.

Table 5: Higher is better. MedMNIST3D test accuracies for a variety of models and symmetry groups. We show the mean accuracy over 5 runs, with std. dev. in brackets. Parameter counts are given, and we indicate runs using data augmentation. The best statistic in each column is bold.

Group	Model	Aug	Nodule3D	Synapse3D	Organ3D	Par (M)
N/A	CNN	No	0.873 (0.005)	0.716 (0.008)	0.920 (0.003)	00.19
N/A	CNN	Yes	0.879 (0.007)	0.761 (0.008)	0.632 (0.005)	00.19
SO(3)	SCNN	No	0.873 (0.002)	0.738 (0.009)	0.607 (0.006)	00.13
SO(3)	RPP	No	0.801 (0.003)	0.695 (0.037)	0.936 (0.002)	18.30
SO(3)	PSCNN	No	0.871 (0.001)	0.770 (0.030)	0.902 (0.006)	04.17
O(3)	SCNN	No	0.868 (0.009)	0.743 (0.004)	0.902 (0.006)	00.19
O(3)	RPP	No	0.810 (0.013)	0.722 (0.023)	0.940 (0.006)	29.30
O(3)	PSCNN	No	0.873 (0.008)	0.769 (0.005)	0.905 (0.004)	03.51
S4	Ours	Yes	0.887 (0.005)	0.770 (0.002)	0.642 (0.056)	00.19

Table 5 shows classification accuracies on MedMNIST3D for different models and groups. For Nodule and Synapse, our method is comparable or outperforms other architectures, while having fewer parameters. For Organ our method is not competitive; we suggest this is explained by the effect of augmentation, noting that the unaugmented baseline CNN model significantly outperforms its augmented counterpart. However, our model does outperform the augmented baseline.

6.3 Autoregression Task, SMOKE, $G = C_4$

We evaluate our method on the SMOKE dataset, generated with PhiFlow [9] by Wang et al. [21] (see Figure 2 for a visualisation). It consists of smoke simulations with varying initial conditions and external forces, presented as grids of (x, y) components of a velocity field. Following other authors, we use the symmetry group C_4 , acting by 90-degree rotations. Here, the task is to autoregressively predict the next 6 frames of a smoke simulation given the starting 10 frames only: the model uses frames f_i, \dots, f_{i+9} to predict f_{i+10} for $i \in \{0, \dots, 5\}$. Smoke dynamics are affected by buoyancy which is not rotationally equivariant; as a result, this task is only approximately equivariant.

We use the same CNN based architecture as the original authors [21], and the same training and evaluation setup. The input consists of frames containing the (x, y) components of a velocity field, and so as well as rotating each image, we must also reorient the velocity field. Because latent space has the same geometric structure as the input data, i.e. $\mathcal{Z} = \mathbb{R}^c \times \mathbb{R}^h \times \mathbb{R}^w$ (channels \times height \times width), we choose a representation of C_4 given by the regular representation in each channel separately.

Table 6: Lower is better. Test RMSE on the SMOKE dataset for different models on two tasks. We show the mean error over 3 runs, with standard deviation in brackets. Parameter counts are given, and we indicate runs using data augmentation. The best statistic in each column is bold.

Group	Model	Aug	Future	Domain	Par (M)
N/A	CNN	No	0.81 (0.01)	0.63 (0.00)	0.25
N/A	CNN	Yes	0.83 (0.03)	0.67 (0.06)	0.25
N/A	MLP	No	1.38 (0.06)	1.34 (0.03)	8.33
C4	E2CNN	No	1.05 (0.06)	0.76 (0.02)	0.62
C4	RPP	No	0.96 (0.10)	0.82 (0.01)	4.36
C4	Lift	No	0.82 (0.01)	0.73 (0.02)	3.32
C4	RGroup	No	0.82 (0.01)	0.73 (0.02)	1.88
C4	RSteer	No	0.80 (0.00)	0.67 (0.01)	5.60
C4	PSCNN	No	0.77 (0.01)	0.57 (0.00)	3.12
C4	Ours	Yes	0.78 (0.01)	0.61 (0.01)	0.25

We evaluate each model on two metrics: Future, where the test set contains future extensions of instances in the training set; and Domain, where the test and training sets are from different instances.

Table 6 shows the test RMSE for each model on both metrics. All reported figures are imported from the original authors [21], except for ours, augmented CNN, and non-augmented CNN, for which we tune the learning rate. Our method outperforms all models except for PSCNN, which has slightly better scores, with more than 12 times the number of parameters. While our method uses the augmented training set, we note from comparing the two CNN baselines that this gives little advantage for this task. As the task is only approximately equivariant, augmentations introduce noise in the labels, which our model appears to handle well.

7 Limitations and Future Work

Our method is restricted to finite groups; extending it to infinite groups will be an interesting challenge due to the different behaviour of regular representations in that setting. Additionally, our method requires augmenting the training set, which can be computationally expensive for certain data types, such as video, and which can in rare cases be detrimental. We would like to explore how this methodology could enable data augmentation in the latent space, while requiring augmentation of only a subset of the data at training time. More theoretical work is required to understand the preference of the model for the regular representation. Future work could investigate the relationship between our results and the theory of *disentangled representation learning*, starting from its group theoretic formulation due to Higgins et al. [8], widely adopted in the literature [1, 17, 22, 23, 26].

8 Conclusions

In this work, we first explore learnable linear representations on the latent space, using an algebra loss to ensure a high-quality representation, and an equivariance loss to ensure the latent representation is maximally equivariant with the representations on the input and output spaces. We find that for a variety of architectures, tasks and datasets, the models prefer to learn a multiple of the regular representation on the latent space. This informs our new model, which fixes a multiple of the regular representation on the latent space, and adds terms to the loss function that encourages the encoder and decoder to create strong equivariance between input, latent and output spaces. We benchmark our method against a variety of architectures, demonstrating competitive or improved results on a range of tasks, often with lower parameter counts than other models.

References

- [1] Hugo Caselles-Dupré, Michael Garcia-Ortiz, and David Filliat. Symmetry-based disentangled representation learning requires interaction with environments, 2019. [arXiv:1904.00243](#).
- [2] Taco S. Cohen and Max Welling. Steerable CNNs, 2016. [arXiv:1612.08498](#).
- [3] Li Deng. The MNIST database of handwritten digit images for machine learning research. *IEEE Signal Processing Magazine*, 29(6):141–142, 2012.
- [4] Emilien Dupont, Miguel Angel Bautista, Alex Colburn, Aditya Sankar, Carlos Guestrin, Josh Susskind, and Qi Shan. Equivariant neural rendering, 2020. [arXiv:2006.07630](#).
- [5] Marc Finzi, Gregory Benton, and Andrew G Wilson. Residual pathway priors for soft equivariance constraints. In M. Ranzato, A. Beygelzimer, Y. Dauphin, P.S. Liang, and J. Wortman Vaughan, editors, *Advances in Neural Information Processing Systems*, volume 34, pages 30037–30049. Curran Associates, Inc., 2021. URL: https://proceedings.neurips.cc/paper_files/paper/2021/file/fc394e9935fbd62c8aedc372464e1965-Paper.pdf.
- [6] William Fulton and Joe Harris. *Representation Theory*. Springer New York, 2004. doi: 10.1007/978-1-4612-0979-9.

- [7] Yacov Hel-Or and Patrick C Teo. Canonical decomposition of steerable functions. *Journal of Mathematical Imaging and Vision*, 9:83–95, 1998.
- [8] Irina Higgins, David Amos, David Pfau, Sébastien Racanière, Loïc Matthey, Danilo Rezende, and Alexander Lerchner. Towards a definition of disentangled representations, 2018. [arXiv:1812.02230](#).
- [9] Philipp Holl, Vladlen Koltun, Kiwon Um, and Nils Thuerey. PhiFlow: A differentiable PDE solving framework for deep learning via physical simulations. In *NeurIPS workshop*, volume 2, 2020.
- [10] Philip Holmes. *Turbulence, coherent structures, dynamical systems and symmetry*. Cambridge University Press, 2012.
- [11] Gordon James and Martin Liebeck. *Representations and Characters of Groups*. Cambridge University Press, 2001. doi:10.1017/cbo9780511814532.
- [12] Yinzhu Jin, Aman Shrivastava, and Tom Fletcher. Learning group actions on latent representations. In *The Thirty-eighth Annual Conference on Neural Information Processing Systems*, 2024. URL: <https://openreview.net/forum?id=HGNTcy4eEp>.
- [13] Diederik P. Kingma and Jimmy Ba. Adam: A method for stochastic optimization, 2017. URL: <https://arxiv.org/abs/1412.6980>, [arXiv:1412.6980](#).
- [14] Alex Krizhevsky. Learning multiple layers of features from tiny images. 2009. URL: <https://api.semanticscholar.org/CorpusID:18268744>.
- [15] Yann LeCun and Yoshua Bengio. *Convolutional networks for images, speech, and time series*, page 255–258. MIT Press, Cambridge, MA, USA, 1998.
- [16] Nimish Magre and Nicholas Brown. Typography-MNIST (TMNIST): an MNIST-style image dataset to categorize glyphs and font-styles, 2022. [arXiv:2202.08112](#).
- [17] Robin Quessard, Thomas Barrett, and William Clements. Learning disentangled representations and group structure of dynamical environments. *Advances in Neural Information Processing Systems*, 33:19727–19737, 2020. [arXiv:2002.06991](#).
- [18] Christopher Shorten and Taghi M. Khoshgoftaar. A survey on image data augmentation for deep learning. *Journal of Big Data*, 6:60, 2019. doi:10.1186/s40537-019-0197-0.
- [19] Lars Veefkind and Gabriele Cesa. A probabilistic approach to learning the degree of equivariance in steerable CNNs. In *41st International Conference on Machine Learning (ICML 2024)*, 2024. URL: <https://openreview.net/forum?id=49vHLSxjzy>, [arXiv:2406.03946](#).
- [20] Dian Wang, Robin Walters, Xupeng Zhu, and Robert Platt. Equivariant Q learning in spatial action spaces. In *5th Annual Conference on Robot Learning*, 2021. URL: <https://openreview.net/forum?id=IScz42A3iCI>.
- [21] Rui Wang, Robin Walters, and Rose Yu. Approximately equivariant networks for imperfectly symmetric dynamics. In *International Conference on Machine Learning*, pages 23078–23091. PMLR, 2022. [arXiv:2201.11969](#).
- [22] Tan Wang, Zhongqi Yue, Jianqiang Huang, Qianru Sun, and Hanwang Zhang. Self-supervised learning disentangled group representation as feature. *Advances in Neural Information Processing Systems*, 34:18225–18240, 2021. [arXiv:2110.15255](#).
- [23] Xin Wang, Hong Chen, Si’ao Tang, Zihao Wu, and Wenwu Zhu. Disentangled representation learning, 2024. [arXiv:2211.11695](#).
- [24] Maurice Weiler and Gabriele Cesa. General $E(2)$ -Equivariant Steerable CNNs. In *Conference on Neural Information Processing Systems (NeurIPS)*, 2019. [arXiv:1911.08251](#).

- [25] Jiancheng Yang, Rui Shi, Donglai Wei, Zequan Liu, Lin Zhao, Bilian Ke, Hanspeter Pfister, and Bingbing Ni. Medmnist v2 - a large-scale lightweight benchmark for 2d and 3d biomedical image classification. *Scientific Data*, 10(1), January 2023. doi:10.1038/s41597-022-01721-8.
- [26] Tao Yang, Xuanchi Ren, Yuwang Wang, Wenjun Zeng, and Nanning Zheng. Towards building a group-based unsupervised representation disentanglement framework, 2022. arXiv:2102.10303.

A Code

The code to run all the experiments in this paper is available at the following location:

- <https://github.com/rick-ali/parameter-free-approximate-equivariance>

In the README file, we provide instructions to run the code and reproduce the results.

B Exploratory experiments

Here we give details of the exploratory experiments we describe in Section 4. These use the TMNIST, MNIST and CIFAR10 datasets to determine the optimal representation on the latent space. Sections B.1, B.2 and B.3 provide details of the architectures and regularisation terms used for each of these experiments. In all runs, we use the Adam optimiser [13] with default parameters $(\beta_1, \beta_2) = (0.9, 0.999)$, and report additional hyperparameters in Table 7. These were chosen through a manual tuning process.

Table 7: Hyperparameters for exploratory experiments.

Experiment	Latent Dimension	λ_a	λ_t	λ_e	Learning Rate	Batch Size
TMNIST D_1	42	1.0	0.025	0.475	0.003	64
MNIST D_3	30	0.5	0.495	0.005	0.003	64
CIFAR10 C_4	64	1.0	0.25	0.25	0.003	64

B.1 TMNIST autoencoder, $G = D_1$

This experiment uses the TMNIST dataset [16] of digits rendered in a variety of typefaces. We select a data subset corresponding to just two typefaces ‘IBM Plex Sans-MediumItalic’ and ‘Bahianita-Regular’, and augment with random scaling in $[0.8, 1.2]$ centred on the origin, and rotations with angle $\theta \in [-90, 90]$ also centred on the origin. We give some examples of our augmented dataset in Figure 5. The group we use here is $D_1 = \{1, a \mid a^2 = 1\}$ and, for a data point x , we define the group action $\rho_{\mathcal{X}}(a)(x)$ to be the data point with the font swapped, but the rotation and scaling unchanged. In particular, with reference to images Figure 5(i)–(iv), we have $\rho_{\mathcal{X}}(a)(i) = (ii)$, $\rho_{\mathcal{X}}(a)(ii) = (i)$, $\rho_{\mathcal{X}}(a)(iii) = (iv)$ and $\rho_{\mathcal{X}}(a)(iv) = (iii)$. For this experiment we set $L_{\text{task}} = \text{MSE}$, and we use a simple CNN autoencoder with hyperparameters given in Table 7. The architecture is as follows, given in PyTorch syntax.

```
# ----- Encoder -----
nn.Conv2d(in_channels=1, out_channels=int(latent_dim/2),
          kernel_size=3, stride=2, padding=1),
nn.ReLU(),
nn.Conv2d(int(latent_dim/2), latent_dim, kernel_size=3, stride=2, padding=1),
nn.ReLU(),
```

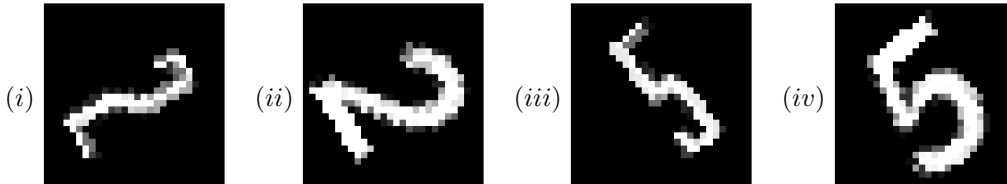


Figure 5: Examples of our augmented training dataset for the TMNIST experiment, from the chosen fonts ‘Bahianita-Regular’ (i), (iii) and ‘IBM Plex Sans-MediumItalic’ (ii), (iv).

```

nn.Conv2d(latent_dim, int(latent_dim*2), kernel_size=7),
nn.ReLU(),
nn.Flatten(),
nn.Linear(int(latent_dim*2), latent_dim)

# ----- Decoder -----
nn.Linear(latent_dim, int(latent_dim*2)),
nn.Unflatten(batch_size, int(self.latent_dim*2), 1, 1),
nn.ConvTranspose2d(in_channels=int(latent_dim*2), out_channels=latent_dim, kernel_size=7),
nn.ReLU(),
nn.ConvTranspose2d(latent_dim, int(latent_dim/2), kernel_size=3, stride=2,
                    padding=1, output_padding=1),
nn.ReLU(),
nn.ConvTranspose2d(int(latent_dim/2), 1, kernel_size=3, stride=2, padding=1, output_padding=1)
nn.Sigmoid()

```

We use the following regularisation term:

$$\text{REG}_{D_1,d} = \text{MSE}(\hat{\rho}_{\mathcal{Z}}(a), \hat{\rho}_{\mathcal{Z}}(a)^{-1}) \quad (6)$$

Here $\hat{\rho}_{\mathcal{Z}}(a)^{-1}$ is computed with $\hat{\rho}_{\mathcal{Z}}(a)^{-1} = \text{torch.linalg.solve}(\hat{\rho}_{\mathcal{Z}}(a), \text{I}_d)$ for efficiency and numerical stability. We found empirically that this regularisation helps to stabilise the training of $\hat{\rho}_{\mathcal{Z}}(a)$, allowing us to achieve lower values for the algebra loss.

B.2 MNIST autoencoder, $G = D_3$

This experiment uses the MNIST dataset [3] of handwritten digits. The group considered is $D_3 = \{e, r, r^2, r^3, s, rs \mid r^3 = e, s^2 = e, rsrs = e\}$, and on the input space we define the group action such that $\rho_{\mathcal{X}}(r)(x)$ is the counterclockwise rotation of x by 60 degrees, and $\rho_{\mathcal{X}}(s)(x)$ is the image generated by flipping x about the vertical axis. For this experiment, we set $L_{\text{task}} = \text{MSE}$, and use a simple MLP autoencoder with hyperparameters given in Table 7. The architecture is specified below in PyTorch syntax.

```

# ----- Encoder -----
nn.Flatten(),
nn.Linear(28*28, 512),
nn.ReLU(),
nn.Linear(512, 256),
nn.ReLU(),
nn.Linear(256, 128),
nn.ReLU(),
nn.Linear(128, latent_dim)

# ----- Decoder -----
nn.Linear(latent_dim, 128),
nn.ReLU(),
nn.Linear(128, 256),
nn.ReLU(),
nn.Linear(256, 512),
nn.ReLU(),
nn.Linear(512, 28*28),
nn.Sigmoid(),
nn.Unflatten(dim=1, unflattened_size=(1, 28, 28))

```

We use the following regularisation term:

$$\text{REG}_{D_3,d} = -0.995 \text{MSE}(\hat{\rho}_{\mathcal{Z}}(r)\hat{\rho}_{\mathcal{Z}}(s)\hat{\rho}_{\mathcal{Z}}(r)\hat{\rho}_{\mathcal{Z}}(s), \text{I}_d) \quad (7)$$

We determined empirically that this regularisation dampens the interaction between the matrices $\hat{\rho}_{\mathcal{Z}}(r)$ and $\hat{\rho}_{\mathcal{Z}}(s)$ in a way that improves training. Low final values of the algebra loss reported in Table 2 give evidence that we still obtain a high-quality representation despite this damping.

B.3 CIFAR10 classifier, $G = C_4$

This experiment uses the CIFAR10 dataset [14] of 32x32 images organised in 10 classes: airplane, automobile, bird, cat, deer, dog, frog, horse, ship, truck. The group considered is the cyclic group of size four C_4 of addition on the set $\{0, 1, 2, 3\}$ modulo 4. The element 1 is a generator for this group, and for an input vector x , we define the group action such that $\rho_{\mathcal{X}}(1)(x)$ is the rotation of x by 90 degrees counterclockwise. For this experiment we set $L_{\text{task}} = \text{CrossEntropy}$, and use a simple CNN classifier with hyperparameters given in Table 7. The architecture is specified below in PyTorch syntax.

```
# ----- Encoder -----
c_hid = 32
nn.Conv2d(3, c_hid, kernel_size=3, padding=1, stride=2),
nn.GELU(),
nn.Conv2d(c_hid, c_hid, kernel_size=3, padding=1),
nn.GELU(),
nn.Conv2d(c_hid, 2*c_hid, kernel_size=3, padding=1, stride=2),
nn.GELU(),
nn.Conv2d(2*c_hid, 2*c_hid, kernel_size=3, padding=1),
nn.GELU(),
nn.Conv2d(2*c_hid, 2*c_hid, kernel_size=3, padding=1, stride=2),
nn.GELU(),
nn.Flatten(),
nn.Linear(2*16*c_hid, latent_dim)

# ----- Classifier -----
nn.Linear(latent_dim, 10)
```

The regularisation term used is the following:

$$\text{REG}_{C_4, d} = \text{MSE}(\hat{\rho}_{\mathcal{Z}}(1)^3, \hat{\rho}_{\mathcal{Z}}(1)^{-1}) \quad (8)$$

Here, $\hat{\rho}_{\mathcal{Z}}(1)^{-1}$ is computed with $\hat{\rho}_{\mathcal{Z}}(1)^{-1} = \text{torch.linalg.solve}(\hat{\rho}_{\mathcal{Z}}(1), \text{I}_d)$ for efficiency and numerical stability. We determined empirically that this regularisation helps to stabilise the training of $\hat{\rho}_{\mathcal{Z}}(1)$ and the behaviour of its inverse.

C Main experiments

Here we give details of the main experiments we describe in Section 6, which test our model of Section 5 on tasks using the DDMNIST, MedMNIST and SMOKE datasets. Sections C.1, C.2 and C.3 provide details of the datasets, architectures and hyperparameters that we use. In all runs we use the Adam optimiser [13] with default parameters $(\beta_1, \beta_2) = (0.9, 0.999)$, with weight decay set to 0 for DDMNIST and MedMNIST, and set to 4×10^{-4} for SMOKE.

C.1 DDMNIST experiments

Data preparation. We follow closely the setup of the originators Veefkind and Cesa [19]. To generate this dataset, pairs of MNIST 28x28 images are chosen uniformly at random, and independently augmented according to the corresponding group action for $G \in \{C_4, D_1, D_4\}$ as per Table 8. We give an example in Figure 6. To ensure comparability of our results with the original paper, for $G \in \{C_4, D_4\}$ we follow their method of introducing interpolation artefacts by rotating each digit image by a random angle $\theta \in [0, 2\pi)$, and then rotating it back by $-\theta$; for $G = D_1$ these interpolation artefacts are not added, in line with the original paper. Finally, the two images are

concatenated horizontally, and padded so that the final image is 56×56 . In this way, we obtain a dataset of 10,000 images with labels in the set $\{(0, 0), (0, 1), \dots, (9, 9)\}$.

Table 8: Symmetry groups and their actions on DDMNIST.

Group	Group Type	Symmetry Generators	Group Size
C_4	Cyclic	90-degree rotation	4
D_1	Dihedral	Horizontal reflection	2
D_4	Dihedral	Horizontal reflection and 90-degree rotation	8

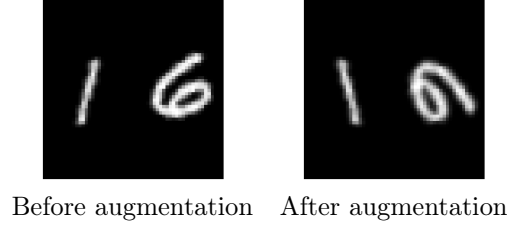


Figure 6: Examples of training data for the DDMNIST experiment with $G = D_4$. The left figure shows concatenated MNIST digits, and the right figure shows the result after a random augmentation. In this instance, the left digit is augmented with a reflection about the vertical axis, and the right digit is augmented with a clockwise 90-degree rotation.

Architecture. We use the same CNN architecture as in Veefkind and Cesa [19], except that the final convolutional layer has an increased number of filters, from 48 to 66. We make this change so that we can fit a copy of the regular representation of $D_4 \times D_4$. To ensure a fair comparison, the results reported in Table 4, including those for SCNN, RPP, etc, are those obtained with the increased number of filters, which we found marginally improved performance. The CNN architecture used is as follows:

```
# ----- CNN -----
n_channels = 1, c = 6, n_classes = 100
torch.nn.Upsample(size=(57, 57)),
torch.nn.Sequential(
    torch.nn.Conv2d(1 * n_channels, c, 7, stride=1, padding=2),
    torch.nn.BatchNorm2d(c),
    torch.nn.ELU(),
),
torch.nn.Sequential(
    torch.nn.Conv2d(c, 2 * c, 5, stride=1, padding=2),
    torch.nn.BatchNorm2d(2 * c),
    torch.nn.ELU(),
),
torch.nn.AvgPool2d(5, stride=2, padding=1),
torch.nn.Sequential(
    torch.nn.Conv2d(2 * c, 4 * c, 3, stride=2, padding=(2,2)),
    torch.nn.BatchNorm2d(4 * c),
    torch.nn.ELU(),
),
torch.nn.AvgPool2d(5, stride=2, padding=1),
torch.nn.Sequential(
    torch.nn.Conv2d(4 * c, 6 * c, 3, stride=2, padding=(0,0)),
    torch.nn.BatchNorm2d(6 * c),
```

```

    torch.nn.ELU(),
),
torch.nn.Sequential(
    torch.nn.Conv2d(6 * c, 6 * c, 3, stride=1, padding=1),
    torch.nn.BatchNorm2d(6 * c),
    torch.nn.ELU(),
),
torch.nn.AvgPool2d(5, stride=1, padding=1),
torch.nn.Conv2d(6 * c, 11 * c, 1),
torch.nn.Flatten(),
torch.nn.BatchNorm1d(11 * c),
torch.nn.ELU(),
torch.nn.Linear(11 * c, n_classes),

```

Hyperparameters. We report the hyperparameters used for the CNN and our model for the DDMNIST experiments in Table 9. These hyperparameters were chosen after a grid search with the following values: learning rate $\in \{0.001, 0.005, 0.0001, 0.0005, 0.00001, 0.00005\}$, and equivariance coupling strength $\lambda \in \{0.5, 1, 1.5, 2\}$. All other hyperparameters match those used by Veefkind and Cesa.

Table 9: Hyperparameters for DDMNIST experiments.

	C_4		D_1		D_4	
	Learning Rate	λ	Learning Rate	λ	Learning Rate	λ
CNN	0.0005	-	0.001	-	0.0005	-
Ours	0.001	2	0.001	1	0.0005	1

C.2 MedMNIST experiments

Data preparation. For this experiment, we use three subsets of the MedMNIST dataset [25], in line with Veefkind and Cesa [19]: Nodule3D, Synapse3D and Organ3D, each containing 3D images of size 28x28x28. Nodule3D is a public lung nodule dataset, containing 3D images from thoracic CT scans; for this dataset, the task is to classify each nodule as benign or malignant. Synapse3D contains 3D images obtained from an adult rat with a multi-beam scanning electron microscope; the task is to classify whether a synapse is excitatory or inhibitory. Organ3D is a classification task for a 3D images of human body organs, with the following labels: liver, right kidney, left kidney, right femur, left femur, bladder, heart, right lung, left lung, spleen and pancreas.

For augmentations, we choose the octahedral group of orientation-preserving rotational symmetries of the cube, which is isomorphic to the permutation group S_4 . We define its action $\rho_X(g)$ on a 3D image x by applying the corresponding rotational symmetry of the cube. Specifically, we parameterise g as a tuple (l, θ) where $l = (x, y, z)$ specifies a rotation axis and θ specifies the rotation angle about the axis l to obtain 24 rotation matrices each with size 3×3 , one for each of the 24 elements of S_4 . In summary, we have rotation matrices corresponding to the following tuples:

- Identity (1 rotation): $(l, 0)$ for any l
- Coordinate-axis rotations (axes through face-centers, 9 rotations): (l, θ) for $l \in \{(1, 0, 0), (0, 1, 0), (0, 0, 1)\}$ and $\theta \in \{\pi/2, \pi, 3\pi/2\}$
- Edge-midpoint-axis rotations (face-diagonal axes, 6 rotations): (l, θ) for $l \in \{(1, 1, 0), (1, -1, 0), (1, 0, 1), (1, 0, -1), (0, 1, 1), (0, 1, -1)\}$ and $\theta \in \{\pi\}$
- Vertex-to-vertex (body-diagonal axes, 8 rotations): (l, θ) for $l \in \{(1, 1, 1), (1, 1, -1), (1, -1, 1), (-1, 1, 1)\}$ and $\theta \in \{2\pi/3, 4\pi/3\}$

Architecture. For these experiments we use the same CNN-based ResNet architecture as Veefkind and Cesa [19]. This is formed from seven 3D convolutional layers, formed into 3 blocks with residual connections, along with batch normalisation and pooling. We specify this in PyTorch syntax as follows.

```
# ----- ResBlock -----
def __init__(self, block, skip):
    super(ResBlock, self).__init__()
    self.block = block
    self.skip = skip

def forward(self, x):
    return self.block(x) + self.skip(x)

# ----- CNN -----
def __init__(self, n_classes, n_channels):
    c=6
    self.upsample = torch.nn.Upsample(size=(29, 29, 29))

    # ----- Resblock 1 -----
    block_1 = torch.nn.Sequential(
        torch.nn.Conv3d(1 * n_channels, c, 7, stride=1, padding=2),
        torch.nn.BatchNorm3d(c),
        torch.nn.ELU(),
    )
    block_2 = torch.nn.Sequential(
        torch.nn.Conv3d(c, 2 * c, 5, stride=1, padding=2),
        torch.nn.BatchNorm3d(2 * c),
        torch.nn.ELU(),
    )
    skip_1 = torch.nn.Sequential(
        torch.nn.Conv3d(1 * n_channels, 2 * c, 7, padding=2)
    )
    self.resblock_1 = ResBlock(torch.nn.Sequential(block_1, block_2), skip_1)

    # ----- Pooling -----
    self.pool_1 = torch.nn.AvgPool3d(5, stride=2, padding=1)

    # ----- Resblock 2 -----
    block_3 = torch.nn.Sequential(
        torch.nn.Conv3d(2 * c, 4 * c, 3, stride=2, padding=(1,1,1)),
        torch.nn.BatchNorm3d(4 * c),
        torch.nn.ELU(),
    )
    pool_2 = torch.nn.AvgPool3d(5, stride=2, padding=1)
    block_4 = torch.nn.Sequential(
        torch.nn.Conv3d(4 * c, 6 * c, 3, stride=2, padding=(2,2,2)),
        torch.nn.BatchNorm3d(6 * c),
        torch.nn.ELU(),
    )
    skip_2 = torch.nn.Sequential(
        torch.nn.AvgPool3d(5, stride=2, padding=0),
        torch.nn.Conv3d(2 * c, 6 * c, 3)
    )
    self.resblock_2 = ResBlock(
        torch.nn.Sequential(block_3, pool_2, block_4), skip_2
    )
```

```

# ----- Resblock 3 -----
block_5 = torch.nn.Sequential(
    torch.nn.Conv3d(6 * c, 6 * c, 3, stride=1, padding=1),
    torch.nn.BatchNorm3d(6 * c),
    torch.nn.ELU(),
)
pool_3 = torch.nn.AvgPool3d(3, stride=1, padding=0)
block_6 = torch.nn.Conv3d(6 * c, 8 * c, 1)
skip_3 = torch.nn.Sequential(torch.nn.Conv3d(6 * c, 8 * c, 3))
self.resblock_3 = ResBlock(
    torch.nn.Sequential(block_5, pool_3, block_6), skip_3
)

# ----- Classifier -----
self.fully_net = torch.nn.Sequential(
    torch.nn.BatchNorm1d(8 * c),
    torch.nn.ELU(),
    torch.nn.Linear(8 * c, n_classes),
)

def forward(self, x):
    x = self.upsample(x)
    x = self.resblock_1(x)
    x = self.pool_1(x)
    x = self.resblock_2(x)
    x = self.resblock_3(x)
    latents = x.reshape(x.shape[0], -1)
    x = self.fully_net(latents)

```

Hyperparameters. We report the hyperparameters used for the baseline with S_4 augmentations, and for our model in the MedMNIST experiments in Table 10. These hyperparameters were chosen after a grid search with the following values: learning rate $\in \{0.001, 0.005, 0.0001, 0.0005, 0.00001, 0.00005\}$, and equivariance coupling strength $\lambda \in \{0.5, 1, 1.5, 2\}$. All other hyperparameters are the same as those used by Veefkind and Cesa.

Table 10: Hyperparameters for MedMNIST experiments.

	Nodule3D		Synapse3D		Organ3D	
	Learning Rate	λ	Learning Rate	λ	Learning Rate	λ
CNN (Augmented)	0.00005	-	0.0001	-	0.0001	-
Ours	0.00005	1	0.0001	1	0.0001	2

C.3 SMOKE experiments

Data preparation. Here we use the SMOKE dataset of Wang et al. [21], which consists of smoke simulations with varying initial conditions and external forces presented as grids of (x, y) components of a velocity field (see Figure 2 for a visualisation). The task is to predict the next 6 frames of the simulation given the first 10 frames only. We evaluate each model on two metrics: Future, where the test set contains future extensions of instances in the training set; and Domain, where the test and training sets are from different instances. We use the Adam optimiser with

We augment the data with the group C_4 , and define the action $\rho_{\mathcal{X}}(g)$ on a frame f as rotation by a multiple of 90 degrees matching the chosen element g , followed by a corresponding reorientation

of the velocity field. The reorientation is necessary to ensure the velocity field remains consistent with the rotation, as exemplified in Figure 7.

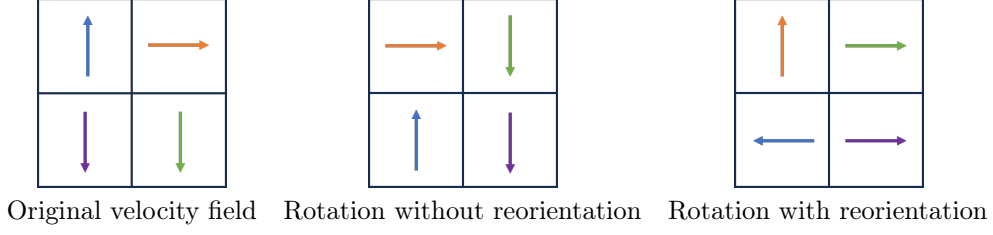


Figure 7: Examples of a velocity field and its augmentations with and without reorientation. Rotating by 90-degrees counterclockwise without reorienting simply moves the spatial grid, but breaks the physical meaning of the underlying system.

Architecture. We use the same CNN architecture as in Veefkind and Cesa [19], which they reproduced from Wang et al. [21], specified as follows:

```
# ----- ConvBlock -----
def __init__(self, in_channels, out_channels, kernel_size):
    self.conv = nn.Sequential(
        nn.Conv2d(in_channels, out_channels, kernel_size,
            padding=(kernel_size - 1) // 2),
        nn.BatchNorm2d(out_channels),
        nn.ReLU(),
    )

def forward(self, x):
    return self.conv(x)

# ----- CNN -----
def __init__(self):
    in_channels = 20, out_channels = 2, hidden_dim = 92, kernel_size = 3, num_layers = 5
    self.layers = [ConvBlock(in_channels, hidden_dim, kernel_size)]
    self.layers += [
        ConvBlock(hidden_dim, hidden_dim, kernel_size)
        for i in range(num_layers - 2)
    ]
    self.layers += [
        nn.Conv2d(
            hidden_dim, out_channels, kernel_size, padding=(kernel_size - 1) // 2
        )
    ]
    self.model = torch.nn.ModuleList(self.layers)

def forward(self, x):
    return self.model(x)
```

Hyperparameters. For both CNN models, with C_4 augmentations and without, and for our model, we use a learning rate of 0.001. Additionally, for our model, we set $\lambda = 0.005$. These hyperparameters were chosen after a grid search with the following values: learning rate $\in \{0.001, 0.005, 0.0001, 0.0005\}$, and equivariance coupling strength $\lambda \in \{0.005, 0.05, 0.5, 1\}$. For all other hyperparameters, we copy the values used by Veefkind and Cesa.